Unsteady Embedded Newton-Busemann Flow Theory

Bing-Gang Tong* and W.H. Hui†
University of Waterloo, Waterloo, Canada

An unsteady, embedded Newton-Busemann flow theory is developed by extending the unsteady Newton-Busemann flow theory of Hui and Tobak to blunt bodies, incorporating the embedded Newtonian flow concept of Seiff and Ericsson. In this theory the unsteady surface pressure includes the Newtonian impact part plus Busemann's centrifugal correction. Applications to dynamic stability of blunt bodies of revolution show that 1) the centrifugal pressure is just as important as the impact part and must not be neglected and 2) with its inclusion the complete theory is in good agreement with existing experiments for high Mach number flow.

Nomenclature

a_n = normal acceleration
c = extended sharp-cone length, or total length of hemisphere-cylinder-flare body
$C_m = M/\frac{1}{2}\rho_\infty U_\infty^2 SL$ = pitching moment coefficient
$C_{m_\theta} = \dfrac{\partial C_m}{\partial \theta}$ = stiffness derivative
$C_{m_{\dot\theta}} = \dfrac{\partial C_m}{\partial(\dot\theta L/U_\infty)}$ = damping-in-pitch derivative
$C_p = (p - p_\infty)/\frac{1}{2}\rho_\infty U_\infty^2$ = pressure coefficient
C_{p_c} = centrifugal pressure coefficient
d = diameter of fore section of cone frustum
$e = \rho_1/\rho_\infty$ = density ratio in primary flowfield of hemisphere-cylinder
e_0, e_1, e_2 = functions defined by Eqs. (17) and (19)
$g = U_1/U_\infty$ = axial velocity ratio in primary flowfield
g_0, g_1, g_2 = functions defined by Eqs. (18) and (19)
h = axial distance from sphere center to pivot axis
K = see Eq. (13)
ℓ_0, ℓ = x coordinate of fore and rear sections of cone frustrum, respectively
L = reference length: extended sharp-cone length c for blunt cone; cylinder diameter $2R_N$ for hemisphere-cylinder-flare
M_∞ = freestream Mach number
p = pressure on ramp surface (or compression surface)
R = radial distance from bow shock centerline to any point on ramp surface (Fig. 1)
R_{sh} = bow shock radius (Fig. 1)
R_B = cone base radius
R_N = spherical nose radius
$r = f(x)$ = body radius
S = reference area: base area for cone; cylinder section area for hemisphere-cylinder-flare
U_∞ = freestream velocity
U_1 = axial velocity component behind the bow shock wave
ΔV_n = difference of normal velocity components before and after impact
X, Y, Z = (with unit vectors $\boldsymbol{I}, \boldsymbol{J}, \boldsymbol{K}$) fixed system of Cartesian coordinates with its origin at sphere center and with $\boldsymbol{I}$ along $\boldsymbol{U}_\infty$
x, y, z = (with $\boldsymbol{i}, \boldsymbol{j}, \boldsymbol{k}$) body-fixed system of Cartesian coordinates with its origin at sphere center and with $\boldsymbol{i}$ along body axis
x, r, ϕ = (with $\boldsymbol{i}, \boldsymbol{e}_r, \boldsymbol{e}_\phi$) body-fixed system of cylindrical coordinates
x_{cg}/c = pivot axis position in proportion to extended sharp-cone length (Fig. 2) or relative to the length of hemisphere-cylinder-flare body
x_i, ϕ_i = position of impact of a particle on secondary shock
ΔY = plunging displacement
$\gamma = \dot Y_0/U_\infty$ = flight-path angle
$\dot\gamma$ = plunging rate
$\epsilon = R_N/R_B$ = bluntness ratio
θ = displacement angle in pitch
$\dot\theta$ = pitching rate
$\kappa(x)$ = curvature of meridian of body surface
σ = angle between body axis and the ray from hemisphere shoulder to the point on ramp (Fig. 1)
τ = ramp cone angle
χ = similarity parameter [Eq. (4)]

Subscripts

1,2 = primary and secondary (embedded) flowfields, respectively
i = functions evaluated at x_i, e.g., $f_i' \equiv \mathrm{d}f(x)/\mathrm{d}x|_{x=x_i}$
n = normal component on body surface
sh = primary bow shock

Superscripts

( ) = dimensional quantity
$\bar{(\ )}$ = nondimensional quantity, normalized by $\bar R_N, \bar\rho_\infty, \bar U_\infty$, respectively (for brevity, overbars omitted from Sec. III.1 onward)

Received Dec. 28, 1984; revision received June 4, 1985.

*Visiting Professor; permanently, Professor and Chairman, Department of Modern Mechanics, University of Science and Technology of China, Hefei, Anhui, China.

†Professor of Applied Mathematics and Mechanical Engineering. Member AIAA.

I. Introduction

RECENTLY, an unsteady Newton-Busemann flow theory has been developed[1-4] and applied to study the aerodynamic stability of airfoils, bodies of revolution, and general three-dimensional shapes flying at very high Mach number M_∞. In particular, it has been shown that 1) the rational limit of gasdynamic theory, as $M_\infty \to \infty$ and the ratio of specific heats $\bar{\gamma} \to 1$, is equivalent to the Newtonian impact flow model plus Busemann centrifugal pressure correction, 2) the centrifugal pressure is just as important as the impact pressure and must not be neglected, and 3) with its inclusion the complete unsteady Newton-Busemann flow theory is in good agreement with experiments on sharp-nosed bodies.

The theory, however, gives poor predictions of stability derivatives of blunt bodies as compared with experimental data for large but finite Mach number M_∞ and for $\bar{\gamma} = 1.4$. As pointed out in Refs. 2 and 4, the reason for this is the inability of the bow shock to closely follow the surface of the blunt body. Mathematically, this is manifested as the existence of a singularity at the stagnation point in the blunt-nose region. Thus, in the steady flow past a blunt body according to Newtonian flow model, the mass of the fluid particles impacted at the stagnation point cumulates to infinity there. This singularity at the stagnation point, which exists in the Newtonian impact flow already, is not remedied by, but persists in, the Busemann centrifugal pressure correction. Such a singularity always exists at the stagnation point in any steady or unsteady Newtonian flow theory but is integrable as shown in Ref. 4. On the other hand, no singularity exists for sharp-nosed or concave shapes, and for such shapes (e.g., a sharp cone) the Newton-Busemann theory, and not the Newtonian theory alone, provides the correct limiting value for high Mach number flow.

The above discussions thus show that steady and unsteady Newton-Busemann flow theory gives a good first approximation to high Mach number flow past sharp-nosed (or sharp-edged) bodies or bodies with small bluntness for which the stagnation region is either nonexistent or small. On the other hand, for blunt bodies for which the stagnation region is dominant, Newton-Busemann flow theory is in serious error, and some empirical method has to be used to account for the fact that the bow shock does not follow the body surface closely. In the steady flow case an empirism[5] is to modify the Newtonian coefficient of 2.0 in the impact pressure formula so as to account for the effects of nose bluntness, finite M_∞, and $\bar{\gamma}$ differing from 1.0, while retaining its value of 2.0 for sharp-edged shapes.

For oscillating vehicles, Ericsson[7] has extended Seiff's[6] steady embedded Newtonian concept to unsteady flow to give simple empirical formulas for predicting the stability of blunt bodies in high Mach number flow. The purpose of this paper is to generalize the embedded Newtonian flow concept of Seiff[6] and Ericsson[7] to extend the unsteady Newton-Busemann flow theory of Hui and Tobak[2] to blunt bodies. In doing so, we will follow the approach of Ericsson[7] but will include the Busemann centrifugal pressure correction so that the resulting unsteady embedded Newton-Busemann flow theory will give a correct value for, and include as a special case, the sharp-nosed body.

It turns out that (Section VII) the centrifugal pressure correction for blunt-nosed bodies is as important as the Newtonian impact part and that with its inclusion the complete theory gives predictions of dynamic stability derivatives of blunt bodies in good agreement with existing experimental data.

II. Problem Formulation

1. Unsteady Embedded Newton-Busemann Flow Concept

We now generalize Seiff's steady embedded Newtonian flow concept[6] to the unsteady flow case including Busemann centrifugal pressure correction. When a ramp or compression surface on the body of revolution with a bow shock generates an attached secondary shock wave with thin shock layer,‡ the unsteady Newton-Busemann flow theory[2] is assumed applicable in the flow behind the secondary shock wave, using the unsteady nonuniform supersonic flowfield behind the primary bow shock as the incoming flow. Accordingly, we have

$$\frac{p_2 - p_1}{\frac{1}{2}\rho_1 U_1^2} = 2\left(\frac{\Delta V_n}{U_1}\right)^2 + \frac{p_c}{\frac{1}{2}\rho_1 U_1^2} \tag{1}$$

The above relation can be written in terms of pressure coefficients based on the freestream parameters

$$C_{p_2} = C_{p_1} + 2\left(\frac{\rho_1}{\rho_\infty}\right)\left(\frac{\Delta V_n}{U_\infty}\right)^2 + C_{p_c} \tag{2}$$

2. The Flow Model

Consider a spherically blunted body of revolution in a uniform supersonic/hypersonic flow performing a harmonic pitching oscillation with zero mean angle of attack about the pivot axis 0 passing through the center of the hemisphere cap (Fig. 1). Simultaneously, the pivot axis 0 at the hemisphere center undergoes a harmonic plunging oscillation with the same frequency as that of pitching. It will be assumed that pitching displacement θ, pitching rate $\dot{\theta}$, plunging rate γ, and plunging acceleration $\dot{\gamma}$ are all $\ll 1$, and all terms of second order and higher will be neglected.

Let the spherically blunted body be composed of a hemisphere-cylinder and ramps or compression surfaces. The problem of calculating the unsteady flow around the body may be reduced to two tasks: 1) calculating the primary flowfield around a hemisphere-cylinder in the combined pitching-plunging motion in the uniform hypersonic flow, and 2) calculating the secondary (embedded) flowfield over the compression surfaces for which the unsteady Newton-Busemann flow theory[2] applies.

For the first task, it is well known[8] that the bow shock wave shape and the primary flowfield of the hemisphere-cylinder are not affected by its afterbody oscillation about the sphere center. Furthermore, as shown in Fig. 1 of Ref. 9, the pressure p_1/p_s is constant over the inner half-radial extent of the cylindrical shock. In the case of very small plunging rate and amplitude, as commonly encountered in stability analysis, it is therefore reasonable to assume that, as a first approximation, C_{p_1} remains unchanged in the plunging oscillation. The calculation of this flowfield is given in the next section. The remaining task is to apply the unsteady Newton-Busemann flow theory[2] for the determination of the unsteady pressure distribution on ramps or compression surfaces that undergo both pitching (around the sphere center) and plunging oscillations in the primary nonuniform steady flowfield of a hemi-

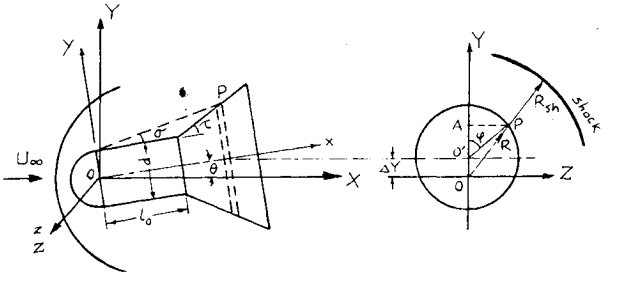

Fig. 1 Configuration showing notation.

‡Here the spherically blunted cone is idealized as the hemisphere-cylinder with the ramp mounted on, where an attached secondary shock wave is assumed.

sphere-cylinder in axial hypersonic flight based on the embedded flow concept.

III. Flow over a Hemisphere-Cylinder in Axial Hypersonic Flight

Following Ericsson,[7] we assume similarity profiles of the shock layer in the primary flowfield, i.e.,

$$\rho_1/\rho_\infty = e(R/R_{sh}), \qquad U_1/U_\infty = g(R/R_{sh}) \tag{3}$$

and introduce a similarity parameter,

$$\chi = \left(\frac{R}{R_N} - 1\right)^2 \Big/ \left(\frac{R_{sh}}{R_N}\right)^2 \tag{4}$$

In the following, all the lengths x, y, z, etc., are scaled by the sphere nose radius R_N, velocity V by U_∞, density ρ_1 by ρ_∞, pressure p by $\rho_\infty U_\infty^2$, and time t by R_N/U_∞. The normalized parameters are written with the overbar, which will be omitted for brevity hereafter, as all quantities concerned afterward are nondimensional.

1. Expression of χ

As shown in Fig. 1,

$$R^2 = (\Delta Y + \overline{\mathcal{O}'A})^2 + \overline{PA}^2 \tag{5}$$

$$\Delta Y = (\Delta Y)_{pitch} + (\Delta Y)_{plunge} \tag{6}$$

$$(\Delta Y)_{pitch} = x\sin\theta \tag{7}$$

$$(\Delta Y)_{plunge} = x\gamma/U_1 \tag{8}$$

where $\gamma = \dot{Y}_0$ is the flight-path angle ($\dot{Z}_0$ in the standard notation) and is also the nondimensional plunging rate of pivot axis $\mathcal{O}$. We also have

$$\overline{PA} = (1 + x\tan\sigma)\sin\phi \tag{9}$$

$$\overline{\mathcal{O}'A} = (1 + x\tan\sigma)\cos\phi\cos\theta \tag{10}$$

where σ is the angle between the body axis and the ray connecting the hemisphere shoulder with a current point on the compression surface (Fig. 1). Substituting Eqs. (6-10) into Eq. (5) and neglecting terms $\mathcal{O}(\theta^2, \gamma^2, \theta\gamma)$, we get

$$(R-1)^2 = x^2\tan^2\sigma[1 + 2(\theta + \gamma/U_1)\cot\sigma\cos\phi] \tag{11}$$

From Swigart's third-order blast-wave theory,[10] the shock wave shape of a hemisphere-cylinder is given in the present case by

$$R_{sh} = 1.124C_{D_N}^{\frac{1}{4}}(x+1)^{\frac{1}{2}}K \tag{12}$$

where

$$K = 1 + \left(0.7865/M_\infty^2 C_{D_N}^{\frac{1}{2}}\right)(x+1) - \left(1.4509/M_\infty^4 C_{D_N}\right)(x+1)^2 \tag{13}$$

and the Newtonian value of $C_{D_N} = 1.0$ is used in Eqs. (12) and (13). Other empirical values could also be used for C_{D_N} but would lead to only very little change in the results for the stability derivatives. We prefer to use the theoretical value $C_{D_N} = 1.0$ in this paper.

Finally, substituting Eqs. (11-13) into Eq. (4), we obtain the desired expression of χ

$$\chi = \frac{x^2\tan^2\sigma}{1.265(x+1)C_{D_N}^{\frac{1}{2}}K^2}\left[1 + 2\left(\theta + \frac{\gamma}{U_1}\right)\cot\sigma\cos\phi\right] \tag{14}$$

2. Empirical Formulas of $\rho_1(\chi)$ and $U_1(\chi)$

Seiff and Whiting's calculated results[9] for a hemisphere-cylinder in hypersonic axial flight in air have been fitted by the following formulas (for $\rho_1 U_1^2 \le 1$ and $U_1 \le 1$):

$$\rho_1 = \begin{cases} e(\chi) = 0.27 + 1.2\chi + 0.15\chi^2 & \chi \le 0.65 \\ 1 & \chi > 0.65 \end{cases} \tag{15}$$

$$U_1 = \begin{cases} g(\chi) = 0.7 + 0.3\chi^{\frac{1}{2}} & \chi \le 0.65 \\ 1 & \chi > 0.65 \end{cases} \tag{16}$$

Equations (15) and (16) for $\chi \le 0.65$ may be further expanded as Taylor series in the variables θ and γ, so that

$$e(\chi) = e_0 + e_1\theta\cos\phi + e_2\gamma\cos\phi \tag{17}$$

$$g(\chi) = g_0 + g_1\theta\cos\phi + g_2\gamma\cos\phi \tag{18}$$

where, as seen from Eqs. (14-16),

$$\chi_0 \equiv \chi|_{\theta=\gamma=0} = x^2\tan^2\sigma/\left[1.265(x+1)C_{D_N}^{\frac{1}{2}}K^2\right] \tag{19a}$$

$$e_0 = e(\chi_0) \tag{19b}$$

$$e_1 = 2\chi_0(1.2 + 0.3\chi_0)/\tan\sigma \tag{19c}$$

$$e_2 = e_1/g_0 \tag{19d}$$

$$g_0 = g(\chi_0) \tag{19e}$$

$$g_1 = 0.3\chi_0^{\frac{1}{2}}/\tan\sigma \tag{19f}$$

$$g_2 = g_1/g_0 \tag{19g}$$

IV. Unsteady Embedded Newtonian Impact Pressure

Following the process of analysis in Hui and Tobak,[2] the normal velocities before and after impact on the embedded shock are

$$(V_n)_{before} = g\boldsymbol{I}\cdot\boldsymbol{n} = -g(\chi)\mu(x)[f'(x) + \cos\phi] \tag{20}$$

$$(V_n)_{after} = \mu(x)\cos\phi\{\dot{\theta}[x + f(x)f'(x)] + \gamma\} \tag{21}$$

where $r = f(x)$ is the equation of the compression surface of the body, and $\mu(x) = [1 + f'^2(x)]^{-\frac{1}{2}}$.

The unsteady embedded Newtonian impact pressure in Eq. (2) is thus expressed as

$$\begin{aligned}(C_p)_{impact} &= 2e[(V_n)_{after} - (V_n)_{before}]^2 \\ &= 2\mu^2 f'[e_0 g_0^2 f' + (\theta + \gamma/g_0)(2e_0 g_0^2 + 2e_0 g_0 g_1 f' \\ &\quad + e_1 g_0^2 f')\cos\phi + 2\dot{\theta}e_0 g_0(x + ff')\cos\phi]\end{aligned} \tag{22}$$

V. Unsteady Embedded Centrifugal Force Correction

We again follow the analysis process of Ref. 2 to determine first the particle trajectories and then the centrifugal force correction.

Fluid particles after impact are subject to move without tangential acceleration. As given by Eqs. (23) and (24) in Ref. 2, the equations governing the motion of the particles are

$$\frac{d}{dt}\left(\frac{\dot{x}}{\mu}\right) + \dot{\gamma}\mu f'\cos\phi = 0 \tag{23a}$$

$$\frac{d}{dt}(f^2\dot{\phi}) - (\dot{\gamma} + 2\theta\dot{x})f\sin\phi = 0 \tag{23b}$$

The initial conditions of the particle in the embedded flowfield at $x = x_i$, $\phi = \phi_i$, $t = t_i$ are

$$(\dot{x}/\mu)_i = \mu_i \left[g_{0i} + \left(\theta + \frac{\gamma}{g_{0_i}}\right)(g_{1i} - f_i' g_{0_i})\cos\phi_i - \dot{\theta}(x_i f_i' - f_i)\cos\phi_i \right] \tag{24a}$$

$$(\dot{\phi} f)_i = \left[(\theta + \gamma/g_{0_i})\, g_{0_i} + \dot{\theta} x_i\right]\sin\phi_i \tag{24b}$$

The solutions to Eqs. (23) and (24) are in the form

$$\dot{x}/\mu = A(x, x_i) + [\theta B(x, x_i) + \dot{\theta} C(x, x_i) + \gamma D(x, x_i) + \dot{\gamma} E(x, x_i)]\cos\phi \tag{25a}$$

$$\dot{\phi} f = [\theta F(x, x_i) + \dot{\theta} G(x, x_i) + \gamma H(x, x_i) + \dot{\gamma} J(x, x_i)]\sin\phi \tag{25b}$$

where

$$A = \mu_i g_{0_i}$$

$$B = \mu_i (g_{1_i} - g_{0_i} f_i')$$

$$C = \left(f_i' - \frac{g_{1_i}}{g_{0_i}}\right)\int_{x_i}^{x} \frac{d\xi}{\mu(\xi)} - \mu_i (x_i f_i' - f_i)$$

$$D = B/g_{0_i}$$

$$E = \frac{(f_i' - g_{2_i})}{g_{0_i}}\int_{x_i}^{x} \frac{d\xi}{\mu(\xi)} + \frac{1}{\mu_i g_{0_i}}[f_i - f(x)]$$

$$F = f_i g_{0_i}/f(x)$$

$$G = \frac{1}{f(x)}\left[f_i x_i - \frac{f_i}{\mu_i}\int_{x_i}^{x} \frac{d\xi}{\mu(\xi)} + 2\int_{x_i}^{x} f(\xi)\, d\xi\right]$$

$$H = F/g_{0_i}$$

$$J = \frac{1}{\mu_i g_{0_i} f(x)}\int_{x_i}^{x} \frac{[f(\xi) - f_i]}{\mu(\xi)}\, d\xi \tag{26}$$

The normal acceleration of the particle after impact is

$$a_n = \mu^3 f''\left(\frac{\dot{x}}{\mu}\right)^2 + 2\dot{\theta}\cos\phi\left(\frac{\dot{x}}{\mu}\right) + \mu\dot{\gamma}\cos\phi \tag{27}$$

Substituting Eqs. (25) and (26) into Eq. (27), we have

$$a_n = \kappa A^2 + 2\cos\phi \times \left[\kappa A B\left(\theta + \frac{\gamma}{g_{0_i}}\right) + A(\kappa C + 1)\dot{\theta} + \left(\kappa A E + \frac{\mu}{2}\right)\dot{\gamma}\right] \tag{28}$$

where $\kappa(x) = \mu^3(x) f''(x)$ is the curvature of the meridian of the compression surface.

Now we seek an expression for $\rho\, dn$ from the law of conservation of mass:

$$\frac{\partial}{\partial t}[\rho\, dn] + \frac{\mu(x)}{f(x)}\frac{\partial}{\partial x}\left[\frac{f(x)\dot{x}}{\mu(x)}\rho\, dn\right] + \frac{1}{f(x)}\frac{\partial}{\partial \phi}[\dot{\phi} f(x)\rho\, dn] = 0 \tag{29}$$

The boundary condition required can be obtained by applying the law of conservation of mass across the shock at the outer edge. The mass flow rate before the shock is

$$dm_1 = f_i \left\{ e_{0_i} g_{0_i} f_i' + \left(\theta + \frac{\gamma}{g_{0_i}}\right)\cos\phi_i (e_{0_i} g_{0_i} + f_i' g_{0_i} e_{1_i} + f_i' e_{0_i} g_{1_i}) + \dot{\theta}\cos\phi_i [e_{0_i}(x_i + f_i' f_i)] \right\} dx_i\, d\phi_i \tag{30}$$

The mass flow rate behind the shock is

$$dm_2 = \left(\frac{\dot{x}}{\mu}\right)_i f_i [\rho\, dn]_i\, d\phi_i \tag{31}$$

From $dm_1 = dm_2$ and after using Eqs. (25a) and (26), we have the boundary condition

$$[\rho i dn]_i = \frac{1}{\mu_i g_{0_i}}\left\{ e_{0_i} g_{0_i} f_i' + \left(\theta + \frac{\gamma}{g_{0_i}}\right)\cos\phi_i \left(\frac{e_{0_i} g_{0_i}}{\mu_i^2} + f_i' g_{0_i} e_{1_i}\right) + \dot{\theta}\cos\phi_i \left(\frac{e_{0_i} x_i}{\mu_i^2}\right)\right\} dx_i \tag{32}$$

The solution to Eq. (29) with the boundary condition (32) is in the form

$$\rho\, dn = \frac{dx_i}{f(x)}\{\alpha(x, x_i) + [\theta\beta(x, x_i) + \dot{\theta}\eta(x, x_i) + \gamma\delta(x, x_i) + \dot{\gamma}\omega(x, x_i)]\cos\phi\} \tag{33}$$

where

$$\alpha = e_{0_i} f_i f_i'/\mu_i$$

$$\beta = -\frac{e_{0_i} f_i^2 f_i'}{\mu_i^2}\int_{x_i}^{x} \frac{d\xi}{\mu(\xi) f^2(\xi)} + \frac{f_i}{\mu_i}\left(\frac{e_{0_i}}{\mu_i^2} + f_i' e_{1_i}\right)$$

$$\eta = -\frac{1}{\mu_i g_{0_i}}\left\{ \alpha\left(f_i' - \frac{g_{1_i}}{g_{0_i}}\right)\int_{x_i}^{x} \frac{d\xi}{\mu(\xi)} + \alpha\int_{x_i}^{x} \frac{d\xi}{\mu(\xi) f^2(\xi)}\left[f_i x_i - \frac{f_i}{\mu_i}\int_{x_i}^{\xi} \frac{d\lambda}{\mu(\lambda)} + 2\int_{x_i}^{\xi} f(\lambda)\, d\lambda\right] - P(x_i)\int_{x_i}^{x} \frac{d\xi}{\mu(\xi)}\int_{x_i}^{\xi} \frac{d\lambda}{\mu(\lambda) f^2(\lambda)} + Q(x_i)\int_{x_i}^{x} \frac{d\xi}{\mu(\xi)} - \frac{e_{0_i} f_i x_i}{\mu_i^2}\right\}$$

$$\delta = \beta/g_{0_i}$$

$$\omega = -\frac{1}{\mu_i g_{0_i}}\left\{ \alpha\frac{(f_i' - g_{2_i})}{g_{0_i}}\int_{x_i}^{x} \frac{d\xi}{\mu(\xi)} + \frac{\alpha}{\mu_i g_{0_i}} \times \left[f_i - f(x) + \int_{x_i}^{x} \frac{d\xi}{\mu(\xi) f^2(\xi)}\int_{x_i}^{\xi} \frac{[f(\lambda) - f_i]}{\mu(\lambda)}\, d\lambda\right] - \frac{P(x_i)}{g_{0_i}}\int_{x_i}^{x} \frac{d\xi}{\mu(\xi)}\int_{x_i}^{\xi} \frac{d\lambda}{\mu(\lambda) f^2(\lambda)} + \frac{f_i}{\mu_i g_{0_i}}\left(\frac{e_{0_i}}{\mu_i^2} + f_i' g_{0_i} e_{2_i}\right)\int_{x_i}^{x} \frac{d\xi}{\mu(\xi)}\right\}$$

and

$$P(x_i) = \frac{e_{0_i} f_i^2 f_i'}{\mu_i^2}$$

$$Q(x_i) = \frac{f_i}{\mu_i}\left(\frac{e_{0_i}}{\mu_i^2} + f_i' e_{1_i}\right) \tag{34}$$

Now we can obtain the unsteady embedded centrifugal pressure increment

$$C_{p_c} = 2\int_P^{P'} a_n \rho \, \mathrm{d}n \tag{35}$$

where P is the point on the body surface where pressure is evaluated and P' is the point at the outer edge of the shock layer across from P.

Substituting Eqs. (28), (33), and (34) into Eq. (35), we have

$$C_{p_c} = R_0(x) + [\theta R_1(x) + \dot{\theta} R_2(x) + \gamma R_3(x) + \dot{\gamma} R_4(x)]\cos\phi \tag{36}$$

where

$$R_0(x) = 2\frac{\kappa(x)}{f(x)}\int_{x_0}^{x} \alpha A^2 \, \mathrm{d}x_i \tag{37a}$$

$$R_1(x) = 2\frac{\kappa(x)}{f(x)}\int_{x_0}^{x} A(A\beta + 2\alpha B)\, \mathrm{d}x_i \tag{37b}$$

$$R_2(x) = 2\frac{\kappa(x)}{f(x)}\int_{x_0}^{x} A(A\eta + 2\alpha C)\, \mathrm{d}x_i + \frac{4}{f(x)}\int_{x_0}^{x} A\alpha \, \mathrm{d}x_i \tag{37c}$$

$$R_3(x) = R_1(x)/g_0 \tag{37d}$$

$$R_4(x) = 2\frac{\kappa(x)}{f(x)}\int_{x_0}^{x} A(A\omega + 2\alpha E)\, \mathrm{d}x_i + 2\frac{\mu(x)}{f(x)}\int_{x_0}^{x} \alpha \, \mathrm{d}x_i \tag{37e}$$

where x_0 denotes the position of the fore section of the compression surface.

If the flow condition before the secondary shock wave becomes exactly the same as the uniform freestream condition, i.e., $C_{p_1} = 0$, $e_0 = g_0 = 1$, $e_1 = e_2 = g_1 = g_2 = 0$, the embedded Newtonian impact pressure, Eq. (22), and the embedded centrifugal pressure, Eq. (36), are reduced to the corresponding results of Ref. 2. This means that the present unsteady embedded Newton-Busemann flow theory for the body of revolution contains as a special case the unsteady Newton-Busemann flow theory of Hui and Tobak.[2]

VI. Stability Derivatives of the Cone Frustum Pitching Around an Arbitrary Pivot Position

In this case we have, for the cone frustum (Fig. 1),

$$r = f(x) = \frac{d}{2} + (x - \ell_0)\tan\tau$$
$$f'(x) = \tan\tau$$
$$\mu(x) = (1 + f'^2)^{-\frac{1}{2}} = \cos\tau$$
$$\kappa(x) = 0 \tag{38}$$

If the cone frustum is pitching around any pivot axis Cg that is located at an arbitrary distance h from the hemisphere center, the relation between $\dot{\theta}$ and γ is as follows:

$$V_{cg} = \dot{\theta} h + \gamma = 0$$

yielding

$$\gamma = -h\dot{\theta} \tag{39}$$

Now the derivatives of pressure coefficients with respect to θ and $\dot{\theta}$ for a cone frustum pitching around an arbitrary axis can be found from Eqs. (22) and (36), after utilizing Eqs. (38) and (39),

$$\left(\frac{\partial C_p}{\partial \theta}\right)_{\text{impact}} = 2\left[e_0 g_0^2 \sin 2\tau + \left(2e_0 g_0 g_1 + e_1 g_0^2\right)\sin^2\tau\right]\cos\phi \tag{40}$$

$$\left(\frac{\partial C_p}{\partial \theta}\right)_{\text{centr}} = 0 \tag{41}$$

$$\left(\frac{\partial C_p}{\partial \dot{\theta}}\right)_{\text{impact}} = 4\left(\frac{R_N}{L}\right)\left\{e_0 g_0\left(x + \frac{d}{4}\sin 2\tau - \ell_0 \sin^2\tau\right)\tan\tau - \frac{h}{2}e_0 g_0 \sin 2\tau - h\left(e_0 g_0 g_2 + \frac{1}{2}e_2 g_0^2\right)\sin^2\tau\right\}\cos\phi \tag{42}$$

$$\left(\frac{\partial C_p}{\partial \dot{\theta}}\right)_{\text{centr}} = 4\left(\frac{R_N}{L}\right)\cos\phi \frac{\tan\tau}{\left(x - \ell_0 + \frac{d}{2}\cot\tau\right)} \times \int_{x_0}^{x} e_0(\xi) g_0(\xi)\left(\xi - \ell_0 + \frac{d}{2}\cot\tau\right)\mathrm{d}\xi \tag{43}$$

where L is the reference length for defining the nondimensional pitching rate and the moment coefficient. Here we take the extended sharp-cone length c as L for the blunt cone and the cylinder diameter $2R_N$ for the hemisphere-cylinder-flare configuration, in accordance with various experimental data.

Applying Eqs. (40-43), we obtain stability derivatives of the cone frustum by integration,

$$-C_{m_\theta} = \frac{\pi}{SL}\int_{\ell_0}^{\ell}\left(\frac{\partial C_p}{\partial \theta}\right)_{\text{impact}} \cdot (x - h + r\tan\tau)\, r\, \mathrm{d}x \tag{44}$$

$$(-C_{m_{\dot{\theta}}})_{\text{impact}} = \frac{\pi}{SL}\int_{\ell_0}^{\ell}\left(\frac{\partial C_p}{\partial \dot{\theta}}\right)_{\text{impact}} \cdot (x - h + r\tan\tau)\, r\, \mathrm{d}x \tag{45}$$

$$(-C_{m_{\dot{\theta}}})_{\text{centr}} = \frac{\pi}{SL}\int_{\ell_0}^{\ell}\left(\frac{\partial C_p}{\partial \dot{\theta}}\right)_{\text{centr}} \cdot (x - h + r\tan\tau)\, r\, \mathrm{d}x \tag{46}$$

It can be shown that in evaluating $(-C_{m_{\dot{\theta}}})_{\text{impact}}$ in Eq. (45) using Eq. (42), the last term in the brace of Eq. (42) contributes to a part of $(-C_{m_{\dot{\theta}}})_{\text{impact}}$ that is equivalent to Ericsson's $(-C_{m_{\dot{\alpha}}})$,[7] and the remainder of Eq. (42) contributes to the other part, equivalent to his $(-C_{m_q})$. For the cone frustum, $\kappa = 0$, hence, $(-C_{m_{\dot{\theta}}})_{\text{centr}}$ comes solely from the rotary motion. Consequently, we note that for the cone-frustum configuration the Busemann dynamic effect shares a definite contribution to the damping-in-pitch derivative $-C_{m_{\dot{\theta}}}$, on which we will focus our attention in Sec. VII.

In the limiting case, as the cone frustum approaches a pointed cone, keeping its rear section (base) fixed, the bluntness ratio ϵ approaches zero and Eq. (19a) can be rewritten in the form

$$\chi_0 = \left(\tan^2\sigma/1.265 C_{D_N}^{\frac{1}{3}} K^2\right)\frac{(x/R_B)}{\epsilon}\left[1 + (R_B/x)\epsilon\right]^{-1} = \left(\tan^2\sigma/1.265 C_{D_N}^{\frac{1}{3}} K^2\right)\left[\frac{1}{\epsilon}\left(\frac{x}{R_B}\right) - 1 + (R_B/x)\epsilon\right] \tag{47}$$

Thus, we see that $\chi_0 \to \infty$ (except $x = 0$) as $\epsilon \to 0$. Now, as mentioned in Eqs. (15) and (16), we put $e_0 = g_0 = 1$ and, hence, $e_1 = e_2 = g_1 = g_2 = 0$ for $\chi_0 > 0.65$. These relations will be satisfied at every point on the pointed-cone surface except the apex. Therefore, the blunt-nose effect due to the bow shock disappears in the limiting case of a pointed cone, and the unsteady embedded Newton-Busemann flow theory devel-

oped above reduces to the unsteady Newton-Busemann flow theory, as the blunt cone approaches the pointed cone, and the results of stability derivatives for the pointed cone given in Ref. 2 are included as a limiting case of the present theory.

VII. Results and Comparisons

In this section we apply the unsteady embedded Newton-Busemann flow theory developed above to predict the dynamic stability derivative of various shapes and compare them with experiments and existing theories.

Figure 2 shows the predicted damping-in-pitch derivative $(-C_{m_\dot{\theta}})$ vs the pivot axis position x_{cg}/c (in proportion to the extended sharp-cone length) for a spherically blunted 10 deg cone with $\epsilon = 0.3$ and $M_\infty = 6.85$. Plotted for comparison are also the numerical computation of Rie et al.[11] and the experimental results of Khalid and East.[12] It is seen that the Busemann centrifugal contribution, which is the difference between the solid curve and the dashed curve in the figure, is important and must not be neglected. It is also seen that with its inclusion the present unsteady embedded Newton-Busemann theory is in reasonable agreement with experiments.

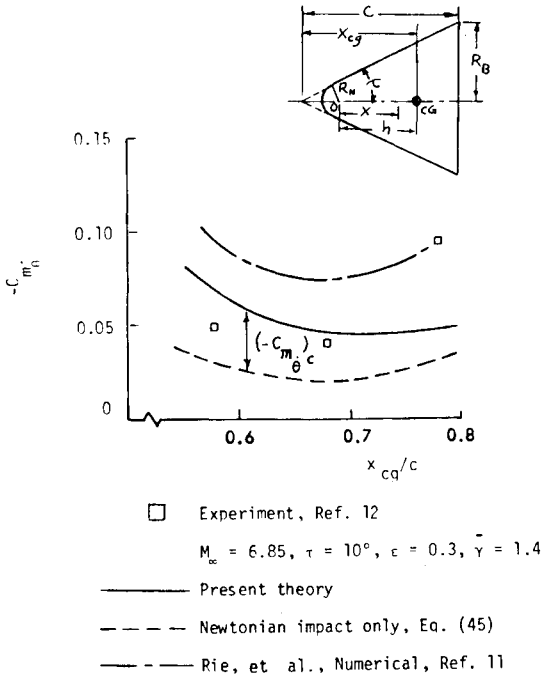

Fig. 2 Damping-in-pitch derivatives vs pivot axis position of a blunted 10 deg cone. $\epsilon = 0.3$, $M_\infty = 6.85$.

Figure 3 shows a compilation of experimental data for $(-C_{m_\dot{\theta}})_{\text{blunt}}/(-C_{m_\dot{\theta}})_{\text{sharp}}$ of cones vs Ericsson's bluntness scaling parameter as presented in Ref. 12. Here the Newton-Busemann value for the sharp-cone damping derivative,[2] which corresponds to the limit of gasdynamic theory, is used as the normalizing factor. The present theoretical results for a 10 deg cone with $x_{cg}/c = 0.6$, $M_\infty = 7$ and for a 5.6 deg cone with $x_{cg}/c = 0.6$, $M_\infty = 14$ are shown in the figure to be also in good agreement with the available experimental data.

In Fig. 4 the present theory is compared to Ericsson's unsteady Newtonian theory[7] in which the centrifugal pressure is neglected. Both results are scaled by the same Newton-Busemann sharp-cone value according to Ref. 2. It is seen that Ericsson's theory is similar to Newtonian impact theory alone and underpredicts the damping derivatives when compared with experimental data (Fig. 3). In passing we note that

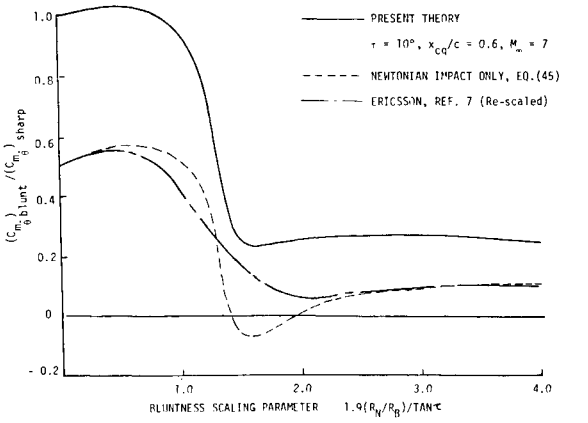

Fig. 4 Contribution of Busemann dynamic effect for blunted cones.

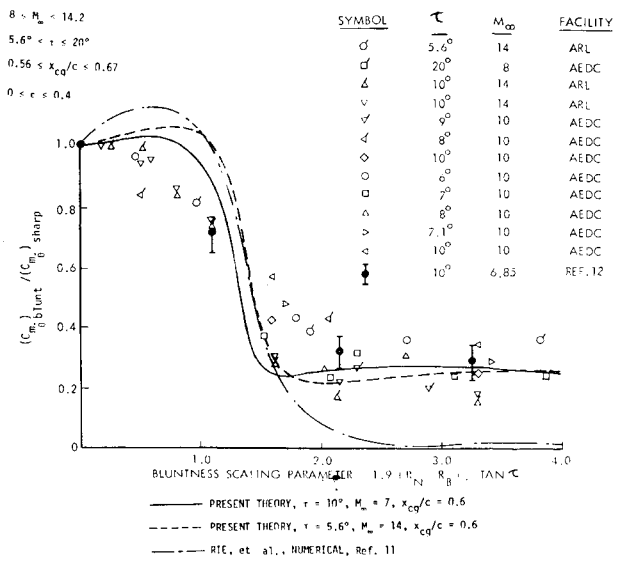

Fig. 3 Normalized damping-in-pitch derivatives vs bluntness scaling parameter for blunted cones.

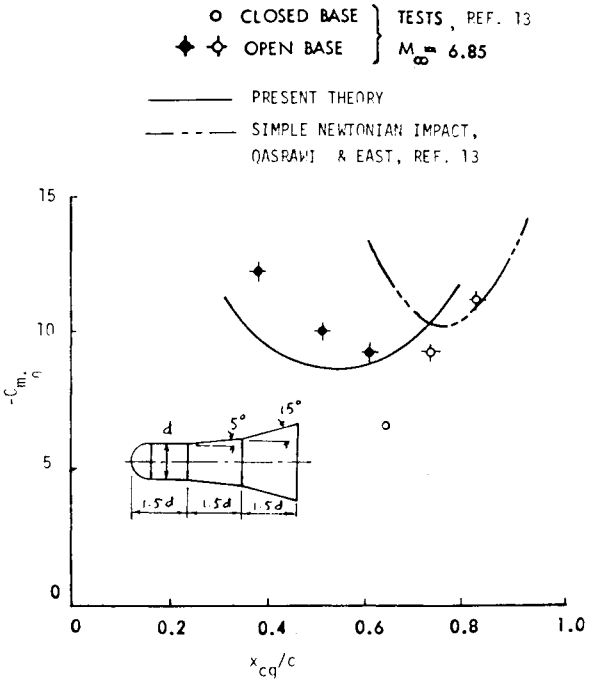

Fig. 5 Damping-in-pitch derivatives vs pivot axis position of AGARD Model HBS.

Ericsson[7] uses the sharp-cone Newtonian value as the scaling factor, which is not the correct limiting value of gasdynamic theory,[14] to show the effects of nose bluntness of the cone and obtained a similar trend (see Fig. 5 of Ref. 12) as in Fig. 3. This seems to suggest that the nose bluntness affects the Newtonian impact part and the Busemann's centrifugal part in the same fashion.

Finally, in Fig. 5 we present the damping-in-pitch derivative $(-C_{m_\theta})$ of the AGARD Model HBS vs pivot axis position for $M_\infty = 7$ together with the experimental data and simple Newtonian impact results of Ref. 13. It is seen that the complete unsteady embedded Newton-Busemann flow theory compares better with experiments for the open base bodies than for the closed base one, although the present theory cannot distinguish the two cases.

VIII. Concluding Remarks

A semiempirical unsteady embedded Newton-Busemann flow theory is developed by extending the unsteady Newton-Busemann flow theory of Hui and Tobak[2] to blunt bodies, incorporating the embedded flow concept of Seiff[6] and Ericsson.[7] It is shown that 1) the Busemann centrifugal effects are important for the dynamic stability derivatives of blunt bodies and must not be neglected, and 2) with its inclusion the complete theory is in good agreement with experiments in high Mach number flow. This agreement of experiments on blunt cones for $(-C_{m_\theta})/(-C_{m_\theta})_{\text{sharp}}$ with the inviscid theory suggests that the viscosity of the fluid affects the blunt-nosed bodies much as it does sharp-nosed bodies, a point first recognized by Ericsson.[7]

Acknowledgments

This work was supported by an International Scientific Exchange Award of the Natural Sciences and Engineering Research Council of Canada. We are indebted to Prof. Li-Xian Zhuang, of the University of Science and Technology of China, for valuable discussions during the course of the research. Thanks are also due Mr. H.J. Van Roessel, of the University of Waterloo, for helping with programming.

References

[1] Hui, W.H. and Tobak, M., "Unsteady Newton-Busemann Flow Theory, Pt. I: Airfoils," *AIAA Journal*, Vol. 19, March 1981, pp. 311-318.

[2] Hui, W.H. and Tobak, M., "Unsteady Newton-Busemann Flow Theory, Pt. II: Bodies of Revolution," *AIAA Journal*, Vol. 19, Oct. 1981, pp. 1272-73 (full paper available from NASA TM-80459).

[3] Hui, W.H. "Unsteady Newton-Busemann Flow Theory, Pt. III: Frequency Dependence and Indicial Response," *Aeronautical Quarterly*, Vol. 33, 1982, pp. 311-328.

[4] Hui, W.H. and Van Roessel, H.J. "Unsteady Newton-Busemann Flow Theory, Pt. IV: Three-Dimensional," *AIAA Journal*, Vol. 22, May 1984, pp. 577-578.

[5] Lees, L., "Hypersonic Flow," *Proceedings of the 5th International Aeronautics Conference*, Los Angeles, Institute of Aeronautics Society, 1955, pp. 241-276.

[6] Seiff, A., "Secondary Flow Fields Embedded in Hypersonic Shock Layers," NASA TN D-1304, 1962.

[7] Ericsson, L.E., "Unsteady Embedded Newtonian Flow," *Astronautica Acta*, Vol. 18, 1973, pp. 309-330.

[8] Rakich, J.W. and Menees, G.P., "Theoretical and Experimental Study of Hypersonic Flow Over Flared Bodies at Incidence," NASA TN D-3218, 1966.

[9] Seiff, A. and Whiting, E.E., "Calculation of Flow Fields from Bow-wave Profiles for the Downstream Region of Blunt-nosed Circular Cylinders in Axial Hypersonic Flight," NASA TN D-1147, 1961.

[10] Swigart, R.J., "Third-over Blast Wave Theory and Its Application to Hypersonic Flow past Blunt-nosed Cylinders," *Journal of Fluid Mechanics*, Vol. 9, Pt. 4, 1960, pp. 613-620.

[11] Rie, H. et al., "Hypersonic Dynamic Stability, Pt. III, Unsteady Flow Field Program," FDL-TDR-64-149, 1967.

[12] Khalid, M. and East, R.A., "Stability Derivatives of Blunt Slender Cones at High Mach Numbers," *Aeronautical Quarterly*, Vol. 30, 1969, pp. 559-599.

[13] Qasrawi, A.M.S. and East, R.A., "Measurements of Dynamic Stability Derivatives of Hyperballistic and Conic Shapes at $M = 6.85$," *Aeronautical Quarterly*, Vol. 32, 1981, pp. 1-30.

[14] Mahood, G.E. and Hui, W.H., "Remarks on Unsteady Newtonian Flow Theory," *Aeronautical Quarterly*, Vol. 27, 1976, pp. 66-74.